Clays and Clay Minerals, Vol. 58, No. 3, 415–430, 2010.

DISSOLUTION OF Cr, Zn, Cd, AND Pb SINGLE- AND MULTI-METAL-SUBSTITUTED GOETHITE: RELATIONSHIP TO STRUCTURAL, MORPHOLOGICAL, AND DEHYDROXYLATION PROPERTIES

NAVDEEP KAUR[1], BALWANT SINGH[1,*], AND BRENDAN J. KENNEDY[2]

[1] Faculty of Agriculture, Food & Natural Resources, The University of Sydney, NSW 2006, Australia
[2] School of Chemistry, The University of Sydney, NSW 2006, Australia

Abstract—The morphology, dehydroxylation, and dissolution properties of single- and multi-metal (Cr, Zn, Cd, and Pb)-substituted goethites prepared using hydrothermal methods are reported. The crystal morphology varied with the nature and the number of metals present in the system. The presence of Cr produced broader crystals while Zn, Cd, and Pb produced narrower crystals than pure goethite. The presence of multiple metals retards the crystal growth of the mineral. Metal substitution caused changes in the unit-cell parameters and the infrared (IR) spectra of the samples. The IR spectra were also sensitive to the morphology of the crystals. The separation of γO and δOH bending frequencies increased with increase in area and aspect ratio of the (100) crystal face. The dissolution-kinetics studies (1 M HCl, 40ºC) of single-metal-substituted goethite provided the following dissolution rate order: Zn- > Pb(II)- $\geqslant$ Pb(IV)- > unsubstituted > Cd- > Cr-goethite. More complex results were obtained for the multi-metal-substituted samples. In the di-metal-substituted goethites, incorporation of Cr suppressed the dissolution rate of Zn-substituted goethite by 85% and Cd suppressed the dissolution rate of Zn-substituted goethite by 53%. Similarly, incorporated Cr and Cd suppressed the dissolution rate of Pb(II)-substituted goethite by 50%. The dissolution rates of multi-metal-substituted goethite were linearly related to the steric strains derived from the lattice parameters of the mineral. Dissolution studies also showed that Cr, Zn, Cd, and Pb(IV) were distributed homogeneously throughout goethite crystals while Pb(II) was enriched in the near-surface regions of the crystals. Incorporation of Cr and Pb(II) increased, while Zn and Pb(IV) decreased the dehydroxylation temperature of single-metal-substituted goethites. Incorporation of Zn suppressed the effect of Cr on the dehydroxylation temperature in multi-metal-substituted goethites.

Key Words—Dehydroxylation, Dissolution Kinetics, Metal-substituted Goethite, Morphology.

INTRODUCTION

Goethite is the most common Fe oxide in soils and metal ores (Singh and Gilkes, 1992). The extraction of metal ores generally causes a multi-elemental contamination of the environment (Dudka and Adriano, 1997). Mine effluents contain metals such as Fe, Cr, Ni, Zn, Cd, Pb, and metalloids such as As. Soils may also be contaminated with a number of metals including heavy metals from industrial effluents, fertilizers, *etc*. (Vega *et al.*, 2004). The co-precipitation of metals with Fe could lead to the simultaneous substitution of various metals into the goethite structure under natural conditions. Natural goethite is usually associated with a number of metals (Gerth, 1990; Singh and Gilkes, 1992; Manceau *et al.*, 2000).

Previous research in the authors' laboratory has shown that simultaneous incorporation of up to 10 mole % Cr, Zn, Cd, and Pb is possible in goethite (Kaur *et al.*, 2009a). The presence of multiple metals in the system affects the preferential order of their entry into the goethite structure and consequently the extent of metal substitution is remarkably different from the single-metal-substituted goethites. The structural properties of the multi-metal-substituted goethites are strongly influenced by the local coordination environments rather than by the ionic radii and valences of the substituent metals.

Establishing the dissolution properties of multi-metal-substituted goethites is very desirable as their dissolution kinetics will determine the rate of release of the substituent metals into solution. Some metals may dissolve rapidly from goethite while others may potentially be locked up for longer periods. The released metals may become bio-available and either essential or toxic to the flora and fauna, depending on the metal's form and concentration. The dissolution properties of Fe oxides, mainly goethite, hematite, and ferrihydrite, are also important as they govern the supply of soluble Fe to plant roots (Schwertmann, 1991). Dissolution studies of single-metal-substituted goethite have shown that the nature of the substituent metal, the extent of metal substitution, and the structural and morphological properties of crystals have important controls on the dissolution rate (Schwertmann, 1991).

Aluminum-, Mn-, Cr-, Co-, and Ni-substituted goethites have been observed to dissolve at very different rates. The incorporation of Al into goethite by either Fe(III)

* E-mail address of corresponding author:
balwant.singh@sydney.edu.au
DOI: 10.1346/CCMN.2010.0580311

(Schwertmann, 1984a, 1991) or Fe(II) (Ruan and Gilkes, 1995) pathways substantially decreased the dissolution rate of goethite in various concentrations of HCl and at different temperatures. Simultaneously substituted (Al, Mn) goethite also showed a slower dissolution rate with increasing levels of Al substitution (Alvarez *et al.*, 2007). Similarly, incorporation of up to 12 mole % Cr reduced the goethite dissolution rate, but to a much greater extent than Al, even at similar levels of incorporation and crystal size (Lim-Nunez and Gilkes, 1987; Schwertmann, 1991). In contrast, incorporation of 0–14 mole % Mn accelerated the rate of dissolution compared to un-substituted goethite (Lim-Nunez and Gilkes, 1987; Schwertmann, 1991; Alvarez *et al.*, 2005; Alvarez *et al.*, 2007). Incorporation of Co also accelerated goethite dissolution, while Ni had no effect (Lim-Nunez and Gilkes, 1987).

The crystal morphology also affects the dissolution rate of goethite. Cornell *et al.* (1974) reported that star-shaped, twinned crystals and large acicular crystals were rapidly attacked along grain boundaries. Pronounced acid attack also occurred at twin planes. The presence of foreign metals also influences the length to width and width to thickness ratios of acicular crystals of goethite. Incorporation of Al made the crystals shorter, broader, thicker, and less domainic (Schulze and Schwertmann, 1984). Structural incorporation of V into goethite increased crystal twinning (Kaur *et al.*, 2009b) whereas substitution of Cu into goethite produced crystal thinning (Huynh *et al.*, 2002). Schwertmann (1984a) found that the presence of Al in the system modified the crystallization conditions and crystal-growth rate, which in turn influenced crystal size and degree of order. Up to 94% of the half-dissolution time (1–96 h) of Al-goethites could be as a result of the variation of the mean crystallite dimension perpendicular to the (110) and (111) planes (Schwertmann, 1984a).

Substituent metals affect the structural properties of goethite due to the differences in their ionic radii, valence, and local bonding environments compared to the Fe^{3+} cation. Schwertmann *et al.* (1985) observed that the dissolution rate of a series of un-substituted goethites synthesized at 4–70ºC ranged between 0.19 and 0.07 min^{-1} m^{-2} g^{-1} and was positively related to the *c* unit-cell parameter (space group *Pnma)*. Despite the similar valency and ionic radius of Mn^{3+} and Fe^{3+} (0.0645 nm for both cations; Shannon, 1976), the accelerated dissolution of Mn-goethite was attributed to the octahedral distortion produced by the Jahn-Teller effect of Mn^{3+} (Alvarez *et al.*, 2007). Substitution of Al^{3+} (0.0535 nm) and Cr^{3+} (0.0615 nm), with ionic radii smaller than that of Fe^{3+}, decreased the dissolution rates of goethite. The decrease was related to increased H-bonding and/or Al/Cr–O–Fe bond strength (Schwertmann, 1984a).

The thermal stability of goethite, as evaluated by the dehydroxylation temperature (Goss, 1987), has been observed to be influenced by particle morphology, crystallinity, and the nature of the substituent metal (Schwertmann, 1984b; Stiers and Schwertmann, 1985; Ford and Bertsch, 1999; Wells *et al.*, 2006). Further, Ford and Bertsch (1999), using high-resolution thermogravimetric analysis, suggested that poorly crystalline goethite shows a single endotherm at low temperature, whereas goethite with a large surface area, with improved crystallinity, shows double/multiple endotherms. Goethite nearly free of structural imperfections shows a single endotherm at high temperature. Wells *et al.* (2006) related the nature of the endotherm to the formation of protohematite.

The present study presents an extension of the work by Kaur *et al.* (2009a), and was undertaken to evaluate the morphology, thermal stability, and dissolution properties of single- and multi-metal (Cr, Zn, Cd, and Pb)-substituted goethites. The relationships between proton dissolution behavior, the extent of metal(s) substitution, and the morphological and structural properties of goethite were also investigated. The study highlights the importance of studying multi-metal-substituted systems *vs.* single-metal-substituted systems.

MATERIALS AND METHODS

Synthesis, chemical composition, and structural analysis

The synthesis technique and chemical composition of pure and metal (Cr, Zn, Cd, and Pb)-substituted goethites were described by Kaur *et al.* (2009a). The unit-cell parameters of pure and metal-substituted goethites, and the local coordination environments of Fe, Cr, Zn, and Pb, were obtained by analysis of synchrotron X-ray diffraction (XRD), extended X-ray absorption fine structure (EXAFS), and X-ray absorption near edge structure (XANES) spectroscopy as described by Kaur *et al.* (2009a).

Morphology

Particle morphology was determined using a CM12 Philips transmission electron microscope (TEM), operated at 120 kV. Samples were prepared by depositing a drop of dilute suspension of goethite on carbon-coated copper grids. Crystal dimensions (length (μm), breadth (μm), and area (μm^2)) were determined from measurements of 100 crystals, using *UTHSCSA Image Tool for Windows* Version 3.00 (Wilcox *et al.*, 1995) and the mean values are reported along with standard errors.

Diffuse reflectance Fourier transform infrared (DRIFT) spectroscopy

DRIFT spectra were obtained using a Bruker-Tensor 37 Fourier transform IR spectrometer. Samples were prepared by mixing and grinding the sample powder with KBr to a final concentration of 1 wt.%. A total of 128 scans were measured in the range 4000–400 cm^{-1} at a resolution of 4 cm^{-1} using pure KBr as the background. Spectral peaks were determined by fitting

https://doi.org/10.1346/CCMN.2010.0580311 Published online by Cambridge University Press

Gaussian and Lorentzian profile functions in *WinXAS* version 2.3 (Ressler, 1998).

Dissolution kinetics

The proton-promoted dissolution rate and congruency of Fe and metal(s) dissolution in single-, di-, tri-, and tetra-metal-substituted goethite were determined by dissolving 25 mg of sample in 60 mL of 1 M HCl in 100 mL HDPE (high-density polyethylene) bottles on an orbital shaker at a cycle of 305 rpm and at 40±1ºC (Cornell *et al.*, 1974). Sample aliquots of 5 mL were withdrawn after 1, 4, 8, 13, 25, 49, 85, 133, 193, 265, 349, and 488 h, filtered immediately through a 0.2 μm membrane, and analyzed for Fe and metals using inductively coupled plasma atomic emission spectroscopy (Varian Vista AX). The proportion of Fe and metal dissolved (wt.%) at a given time was calculated as a fraction of the total amount of Fe or metal present in the sample. As the same procedure was used for both the metal-substituted and pure goethite samples, any effect of decreased acid volume with time on the dissolution kinetics should be similar and was ignored.

Thermo-gravimetric analysis

Thermo-gravimetric analysis (TGA) was performed using a TA Instrument Hi-Resolution TGA 2950 under a N_2 atmosphere flowing at the rate of 40 mL min^{-1}. Approximately 10 mg of sample was heated in a platinum sample pan from ambient temperature to 105ºC at a heating rate of 20ºC min^{-1}, equilibrated at 105ºC for 5 min, and the temperature was then increased to 450ºC at a heating rate of 10ºC min^{-1}.

RESULTS AND DISCUSSION

Morphological analyses of the pure and metal-substituted goethites

Transmission electron microscope images of pure, single-, and multi-metal-substituted goethite samples show rod-shaped crystals in all samples (Figure 1). The crystal lengths showed no trend, which appeared to be independent of the number and type of metals incorporated into goethite (Figure 1, Table 1). Crystal breadth values for single/di/tri-metal-substituted goethite were very similar to the pure (unsubstituted) goethite (0.05 μm); the only exceptions were for Cr-goethite (0.21 μm) and Pb(II)-goethite (0.25 μm) (Figure 1, Table 1). The aspect ratio (breadth/length) of crystals in metal-substituted goethite was greater than for the pure goethite (Table 1). No significant relationship was observed between crystal area or aspect ratio of metal-substituted goethite and the full width at half maximum (FWHM) of the 101 reflection (Table 1). The structures were described in orthorhombic space group *Pnma* as reported by Kaur *et al.* (2009a). Incorporation of Cr, alone or together with Zn, Cd, and Pb, in the goethite structure promoted crystal growth in the crystallographic *X* direction, hampered growth along the *Z* direction, and did not appreciably affect growth in the *Y* direction as compared to pure goethite. Broad and thin lath-shaped

Table 1. Composition and crystal morphology of synthetic single-, di-, tri-, and tetra-metal (Cr, Zn, Cd, and Pb)-substituted goethites.

Sample	Nominal *M* (%)	Structural *M* (%)[a]	Mean crystal length (μm)	Mean crystal breadth (μm)	Mean crystal area (μm^2)	Aspect ratio[b]	$FWHM_{101}$
C_pure goe.	–	–	1.81 (0.31)[c]	0.05 (0.02)	0.09 (0.07)	0.028	0.604
1_Cr	10.00	11.4	1.00 (0.11)	0.21 (0.02)	0.19 (0.02)	0.210	0.848
2_Zn	10.00	11.3	0.68 (0.22)	0.03 (0.01)	0.02 (0.01)	0.044	1.062
3_Cd	10.00	4.3	0.95 (0.31)	0.07 (0.02)	0.08 (0.02)	0.074	0.386
4a_Pb	10.00	2.7	1.32 (0.28)	0.25 (0.07)	0.29 (0.15)	0.189	0.254
4b_Pb[d]	2.00	1.0	0.56 (0.15)	0.04 (0.01)	0.02 (0.01)	0.071	0.924
5_CrZn	5.00 e[e]	6.4	0.88 (0.22)	0.07 (0.02)	0.05 (0.03)	0.074	0.644
6_CrCd	5.00 e	10.5	0.74 (0.26)	0.08 (0.02)	0.06 (0.01)	0.108	0.424
7_CrPb	5.00 e	8.9	0.63 (0.23)	0.09 (0.02)	0.06 (0.03)	0.143	0.444
8_ZnCd	5.00 e	4.9	0.34 (0.17)	0.05 (0.01)	0.02 (0.01)	0.147	0.552
9_ZnPb	5.00 e	4.6	1.27 (0.37)	0.06 (0.02)	0.07 (0.03)	0.047	0.358
10_CdPb	5.00 e	6.6	0.76 (0.29)	0.10 (0.02)	0.08 (0.04)	0.132	0.574
11_CrZnCd	3.33 e	8.7	0.87 (0.08)	0.06 (0.01)	0.05 (0.02)	0.069	0.634
12_CrZnPb	3.33 e	8.3	0.68 (0.11)	0.09 (0.01)	0.07 (0.02)	0.132	0.572
13_CrCdPb	3.33 e	7.7	0.67 (0.14)	0.08 (0.02)	0.06 (0.01)	0.119	0.482
14_ZnCdPb	3.33 e	5.6	0.75 (0.28)	0.05 (0.01)	0.05 (0.01)	0.073	0.456
15_CrZnCdPb	2.50 e	8.0	0.86 (0.26)	0.07 (0.01)	0.06 (0.03)	0.081	0.604

[a] Structural $M = M \times 100/(Fe + M)$ (concentration in moles obtained by total chemical analysis of purified samples)
[b] Aspect ratio = mean breadth/length
[c] Values in parentheses denote the standard error.
[d] The only sample containing Pb in the tetravalent state, all other samples have Pb in the divalent state
[e] Nominal level of each metal.

https://doi.org/10.1346/CCMN.2010.0580311 Published online by Cambridge University Press

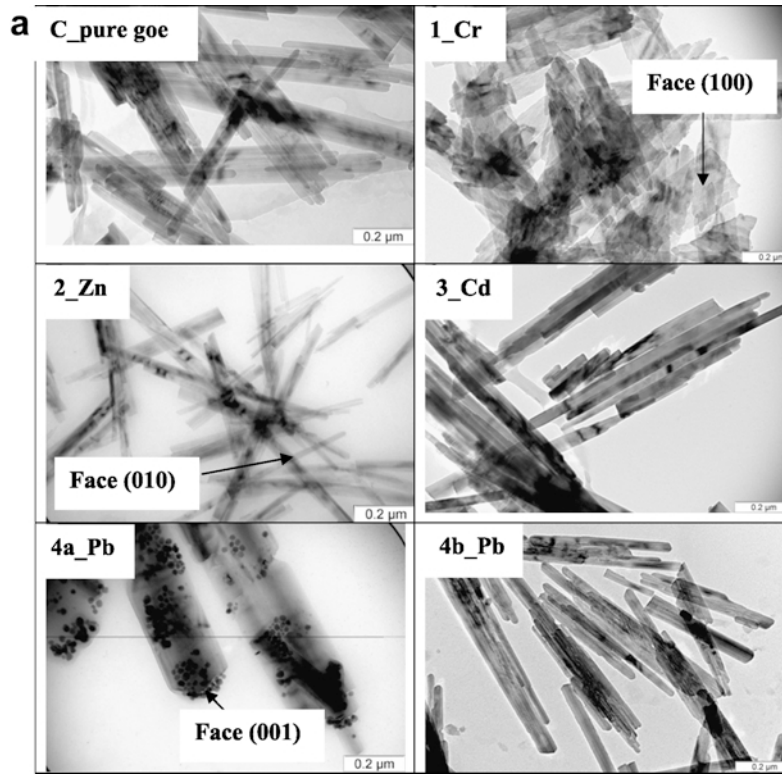

Figure 1. TEM images of synthetic (*above*) a) pure and single-; and (*facing page*) (b) multi-metal (Cr, Zn, Cd, and Pb)-substituted goethite.

goethite crystals were produced (Figure 1, Table 1). The (100) face of the crystals was well developed, whereas the (001) and (010) faces were less well developed in all single- and multi-metal-substituted Cr goethites as compared to pure goethite (Figure 1). Schwertmann *et al.* (1989) observed similar effects for Cr-incorporated goethite (>7 mole %) and concluded that Cr hampered crystal growth at Cr substitution levels above 7 mole %. Similar results were reported for Al substitution in goethite (Schulze and Schwertmann, 1984).

In contrast, Zn and Pb(II) incorporation(s), alone or together, slightly decreased crystal breadth and increased crystal thickness compared to pure goethite, leading to narrow and thick lath-shaped crystals (Figure 1, Table 1). In these crystals, the (100) face was less developed, whereas the (001) and (010) faces were better developed compared to pure goethite (Figure 1). The (001) and (010) faces were not conspicuous in the electron micrographs as observed previously (Atkinson *et al.*, 1968; Cornell *et al.*, 1974) and that was attributed to preferred orientation due to a possible charging effect of the copper grid (Cornell *et al.*, 1974). The (020) faces were poorly developed in all single- and multi-metal-substituted goethite crystals as compared to pure goethite. The results show that the presence of metals inhibits crystal growth along particular faces. The presence of Cr in the multi-element systems has the greatest effect in this regard invariably leading to broader crystals.

Infrared spectroscopy analysis of the pure and metal-substituted goethites

The IR spectrum of goethite contains four features due to the stretching and bending modes of hydroxyl groups, namely out-of-plane (γOH) and in-plane (δOH) bending and symmetrical M-O (τO) and bulk O-H (νOH) stretching. The IR spectra of single- and multi-metal-substituted goethites were similar to that of pure goethite (Table 2, Figure 2) and displayed the four hydroxyl features. The γOH bending frequency ranged from 794.1 to 801.9 cm^{-1}, being smallest for pure goethite and largest for singly Cr-substituted goethite. All substituent metals *viz*. Cr, Zn, Cd, and Pb, either in single- or multi-metal-substituted goethite, increased the γOH bending frequency compared to pure goethite. Schwertmann *et al.* (1989) also observed an increase in the γOH bending frequency of goethite from 793 to 800 cm^{-1} with increasing incorporation of Cr, which they attributed to a shortening of the metal–oxygen bond in the structure due to the replacement of Fe by Cr. Shortening of the Cr–O bond length (1.99 Å) compared to Fe–O (1.96 and 2.11 Å) was observed by EXAFS in Cr-substituted

https://doi.org/10.1346/CCMN.2010.0580311 Published online by Cambridge University Press

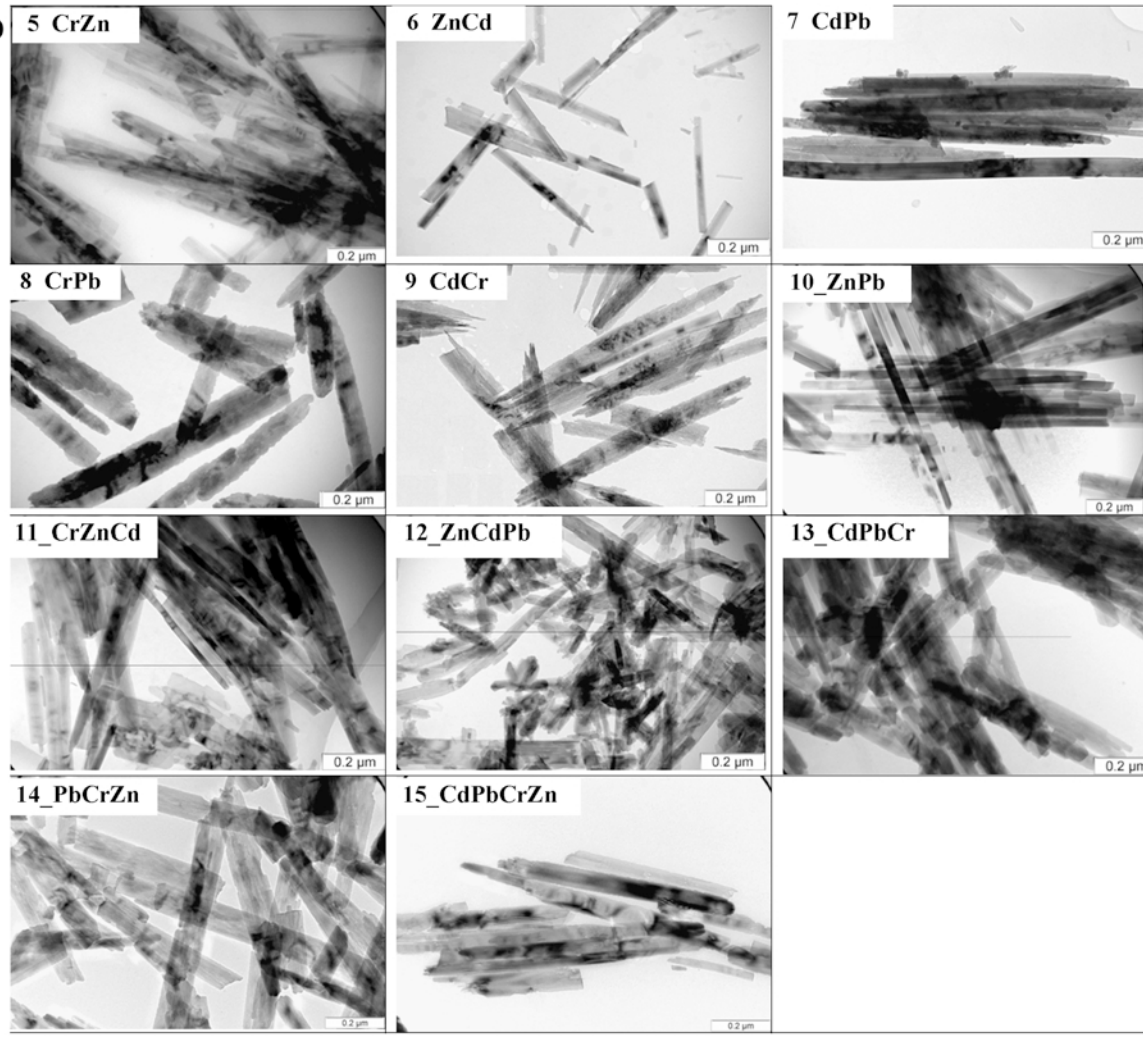

goethite (Singh *et al.*, 2002; Sileo *et al.*, 2004; Kaur *et al.*, 2009a). However, this does not explain the increased γOH bending frequencies observed for Zn, Cd, and Pb incorporations into the goethite structure, as, unlike the Cr–O, the Zn–O (2.25 Å), Cd–O (2.21 Å), and Pb–O (2.15 and 2.31 Å) bond lengths are greater than the Fe–O distance (Kaur *et al.*, 2009a). Clearly, factors other than the average metal–oxygen bond length contribute to changes in the γOH bending frequency. The γOH bending band at 794 cm^{-1} is due primarily to vibrations out of the *b*–*c* plane, *i.e.* along the *a* axis (Schwarzmann and Sparr, 1969). Almost no linear dependency of γOH on total metal substitution in single-, di-, tri-, and tetra-metal substituted goethites (Figure 3a) was observed. Only single Zn-substituted goethite deviates from this trend, which could be related to the extra H^+ present in the structure as a result of the charge-balancing mechanism (Kaur *et al.*, 2009a).

The δOH bending frequency ranged from 888.3 to 898.2 cm^{-1} for single- and multi-metal-substituted goethite and was 894.1 cm^{-1} for pure goethite. Chromium and Zn incorporations decreased it by 6 cm^{-1}, whereas incorporations of either Cd or Pb increased it by 4 cm^{-1} in single-metal-substituted goethite. In multi-metal-substituted goethites, the effects of Cr, Zn, Pb, and Cd incorporation remained the same as for single-metal-substituted goethite. For example, in di-metal substituted goethite, incorporation of both Cd and Pb increased the δOH bending frequency to 897.9 cm^{-1}; Cr and Zn decreased the δOH bending frequency to 890.6 cm^{-1}; and their cross combinations, *e.g.* CrCd, ZnCd, ZnPb, almost neutralized each other's effect and the δOH bending fequency was close to that of pure goethite, 894.10.8 cm^{-1}. Similar results were observed for tri- and tetra-metal-substituted goethites. The increased δOH bending frequency upon incorporation of high-atomic-number cations, *viz.* Cd and Pb, could be attributed to increased repulsion between H^+ and the more positively charged nucleus of Cd and Pb as compared to Fe, Cr, or Zn. The δOH band at 894 cm^{-1} is

https://doi.org/10.1346/CCMN.2010.0580311 Published online by Cambridge University Press

Table 2. Characteristic IR bands and the dehydroxylation temperature for synthetic single-, di-, tri-, and tetra-metal (Cr, Zn, Cd, and Pb)-substituted goethite.

Sample	Frequency (cm^{-1})				DT[e]
	γOH[a]	δOH[b]	δOH-γOH[c]	τO[d]	
C_pure goe.	794.1	894.1	100.0	648.0	283
1_Cr	801.9	891.7	89.8	656.0	305
2_Zn	796.8	888.3	91.5	644.3	231
3_Cd	797.3	898.2	100.9	638.9	282
4a_Pb	797.3	898.2	100.9	638.9	305
5_CrZn	798.4	890.6	92.2	653.6	259
6_CrCd	799.9	894.5	94.6	638.0	277
7_CrPb	799.1	897.9	98.8	643.8	295
8_ZnCd	797.2	894.9	97.7	634.6	277
9_ZnPb	795.5	893.9	98.4	639.2	278
10_CdPb	796.7	897.9	101.2	630.0	286
11_CrZnCd	799.3	893.2	93.9	639.7	274
12_CrZnPb	799.3	892.8	93.5	646.6	276
13_CrCdPb	798.9	893.6	94.7	640.2	282
14_ZnCdPb	796.4	893.6	97.2	636.3	279
15_CrZnCdPb	798.7	897.0	98.3	636.4	294

[a] out-of plane bending mode; [b] in-plane bending mode; [c] degree of separation between in- and out-of plane bending modes; [d] Fe-O symmetric stretching mode; [e] DT-dehydroxylation temperature.

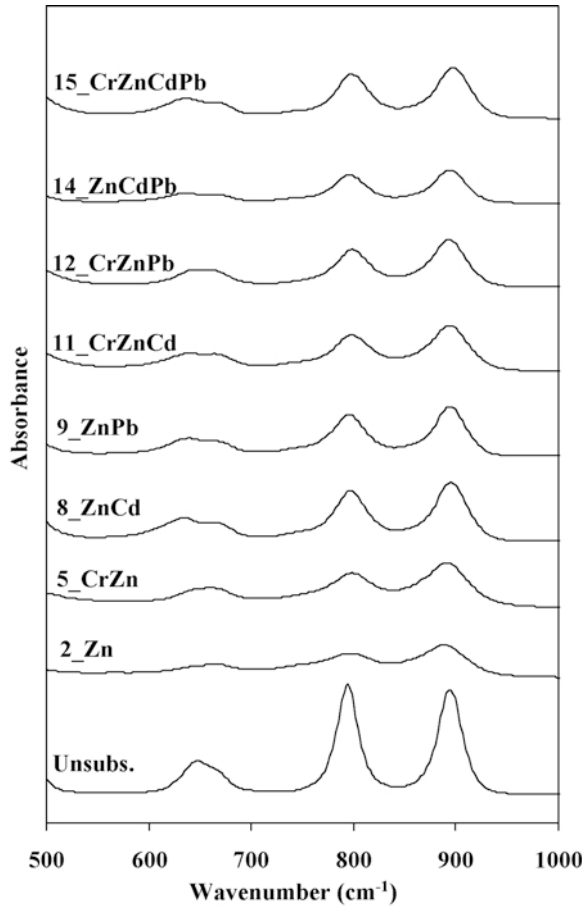

Figure 2. Broadening of the characteristic main IR absorption features of goethite upon substitution of Zn only, and with incorporations of Cr, Cd, and Pb.

primarily due to vibrations in the $b-c$ plane (Schwarzmann and Sparr, 1969). The frequency for the δOH band increased linearly (r^2 = 0.69 − 0.92) with an increase in the unit-cell dimensions above a > 10.00 Å, b > 3.03 Å, and c > 4.62 Å for single-Cd and -Zn, and multi-metal (Cr,Zn)-, (Zn,Cd)-, (Zn,Pb)-, (Cr,Zn,Pb)-, (Zn,Cd,Pb)-, and (Cr,Zn,Cd,Pb)-substituted goethites (Figure 3b). Pure goethite and Cr-, Pb-, (Cr,Cd)-, (Cr,Pb)-, and (Cd,Pb)-substituted goethites had unit-cell dimensions less than these unit-cell values and (Cr,Zn,Cd)- and (Cr,Cd,Pb)-substituted goethites had unit-cell dimensions greater than these values, and fell completely out of the linear trend (Figure 3b). The results show that the frequency for the δOH band is related to both the atomic number of the substituent metal and to the unit-cell dimensions. The latter effect was most obvious in multi-metal-substituted goethites.

An increase in the frequency separation of δOH and γOH, *i.e.* γOH−δOH, is indicative of an increase in the H-bond strength (Primentel and McClellan, 1960; Schulze and Schwertmann, 1984; Schwertmann *et al.*, 1985). The value of γOH−δOH varied from 89.8 to 101.2 cm^{-1} for the present samples (Table 2) and was poorly inversely related (r^2 = 0.53) to total metal substitution (Figure 4a). The results suggest that increasing the total metal substitution decreases the H-bond strength in the goethite structure. Similarly, Schulze and Schwertmann (1984) observed that Al substitution (mole %) alone could explain up to 60% of the variation in the γOH−δOH value for 57 Al-substituted goethite samples. The γOH−δOH value also increased broadly with an increase in area (μm^2) and aspect ratio of the (100) crystal face (Figure 4b), suggesting a relationship

https://doi.org/10.1346/CCMN.2010.0580311 Published online by Cambridge University Press

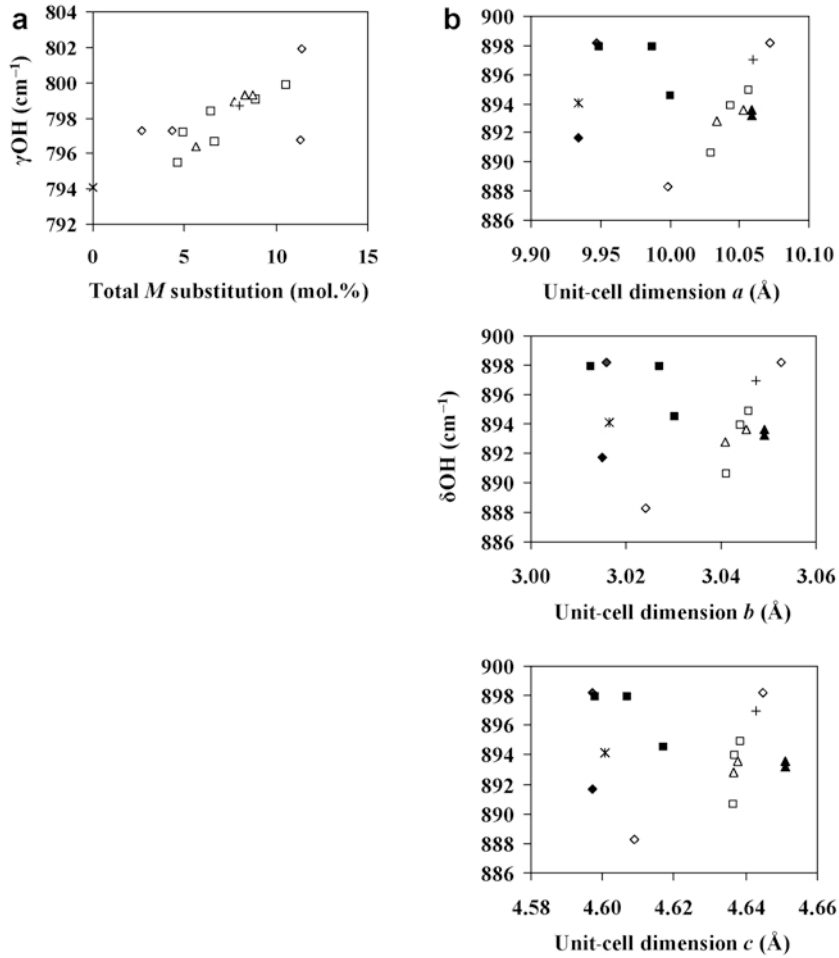

Figure 3. (a) Linear (r^2 = 0.82) relationship of out-of plane (γOH) bending frequency with total substitution in goethite (* pure, ◇ single metal, □ two metals, △ three metals, and + four metals substituted goethite.). The r^2 values are provided excluding the single Zn-substituted sample. (b) Linear (r^2 = 0.69–0.92) relationship of in-plane (δOH) frequency of single Cd- and Zn- and multi-metal (Cr,Zn, Zn,Cd, Zn,Pb, Cr,Zn,Pb, Zn,Cd,Pb, and Cr,Zn,Cd,Pb)-substituted goethite having unit-cell dimensions: a > 10.00 Å, b > 3.03 Å, and c > 4.62 Å. Pure goethite and Cr-, Pb-, Cr,Cd-, Cr,Pb-, and Cd,Pb-substituted goethites having unit-cell dimensions less than the above-mentioned limits and Cr,Zn,Pb and Cr,Cd,Pb having dimensions greater than the above-mentioned do not follow the linear trend (shown with solid symbols for metal-substituted goethite).

between the crystal morphology and the γOH and δOH band frequencies.

The τO stretching frequency ranged from 630 to 656 cm^{-1} for single- and multi-metal-substituted samples (Table 2). The band is known to be influenced by the particle shape of goethite (Cambier, 1986). However, no significant correlation between τO stretching frequency and crystal dimensions was observed for the present samples. Incorporation of Zn in goethite, alone or with other metals (Cr, Pb, Cd), increased the bandwidths and decreased the intensity of all features in the IR spectra (Figure 2), reflecting structural defects or disorder in the crystals (Schwertmann *et al.*, 1985). In general, this effect decreased as the number of different metals substituted along with Zn was increased or as the amount of Zn incorporated decreased (Figure 2, Kaur *et al.*, 2009a). The result is consistent with previous findings of the highly distorted Zn octahedra as revealed by EXAFS (Kaur *et al.*, 2009a).

Dehydroxylation temperature of metal-incorporated and pure goethites

The dehydroxylation temperature of pure goethite was 283ºC, which was further affected by Cr, Zn, Pb(II), and Pb(IV) substitution (Figure 5, Table 2). Incorporation of Cr and, to a lesser extent, Pb(II), increased the dehydroxylation temperature (Figure 5a, Table 2), suggesting that Cr and Pb(II) increased the thermal stability of goethite. Incorporation of Zn, and, to a lesser extent, Pb(IV), decreased the dehydroxylation temperature of goethite (Figure 5a, Table 2). An increase in the dehydroxylation temperature upon Cr

https://doi.org/10.1346/CCMN.2010.0580311 Published online by Cambridge University Press

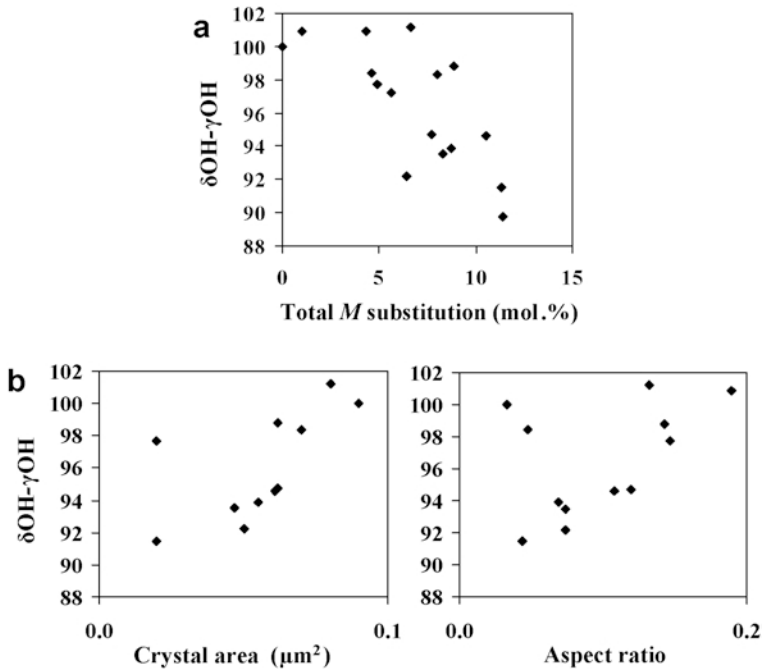

Figure 4. (a) Linear (although poor, $r^2 = 0.53$) relationship of the separation of in-plane (δOH) and out-of plane (γOH) bending frequencies (γOH − δOH), with total metal substitution. (b) The separation of in-plane (δOH) and out-of plane (γOH) bending frequencies (γOH − δOH) *vs.* crystal area (μm^2) and aspect ratio (100 face) of synthetic single-, di-, tri-, and tetra-metal (Cr, Zn, Cd, and Pb)-substituted goethites and pure goethite.

and Al substitution was first reported by Schulze and Schwertmann (1987). Wells (1997) suggested that this could be a consequence of larger *M*−O bond energies, *i.e.* Cr−O (461 kJ/mol) and Al−O (502 kJ/mol) bonds, relative to Fe−O bonds (407 kJ/mol) (Luo and Kerr, 2006−2007). By analogy the lesser thermal stability of Zn-goethite may, in part, reflect the smaller Zn−O (⩽250 kJ/mol) bond energy (Luo and Kerr, 2006−2007). The observed decrease in the H-bond strength, resulting from the incorporation of octahedrally distorted Zn (Kaur *et al.*, 2009a) may also contribute to the thermal instability of Zn goethite.

The substitution of Cd in goethite did not appreciably affect the dehydroxylation temperature (Table 2, Figure 5a), in contrast with the recent work of Huynh *et al.* (2003) who reported such a decrease, an observation that they suggested was a consequence of the smaller Cd−O bond energy, 235.6 kJ/mol *vs.* 407 kJ/mol for Fe−O. The larger crystal sizes obtained in the present study (nearly three times the size of those obtained by Huynh *et al*. (2003) at similar Cd-substitution levels ~4.0 mole %) are suggested here to have counteracted the effect of smaller Cd−O bond energy. Huynh *et al.* (2003) proposed that smaller crystals are expected to lose structural water more easily due to a larger reactive surface area. If this expectation is valid then particle size will impact upon the dehydroxylation temperature.

The magnitude of variation in the dehydroxylation temperature decreased as the number of metals incorporated into goethite increased in the order single-metal- > di-metal- > tri-metal-substitued goethite (Figure 5a,b). The dehydroxylation temperature of di-metal-substituted goethites and pure goethite followed the sequence: CrPb > CdPb ≈ pure goethite > CrCd ≈ ZnPb ≈ ZnCd > CrZn (Table 2, Figure 5b). The dehydroxylation temperature of tri- and tetra-metal-substituted goethites and pure goethite followed the order: CrZnCdPb > CrCdPb ≈ pure goethite > ZnCdPb > CrZnPb > CrZnCd (Table 2, Figure 5b). The trend of the effect of substitutent metals on the dehydroxylation temperature of di- and tri-metal substituted goethites was almost the same as the trend for the single-metal-substituted goethite. The only apparent difference was the effect of Zn which overcame the effect of Cr, as Zn- and Cr-containing di- and tri-metal samples had dehydroxylation temperatures at the lower ends of the above-mentioned trends. This effect was not related to the levels of either Cr or Zn in the (Cr,Zn) goethite as the level of Cr and Zn substitutions were similar (Kaur *et al.*, 2009a). The dominance, in this regard, of Zn over Cr when incorporated into the goethite structure is highlighted.

Dehydroxlation does not occur at a single temperature and, even in pure goethite, two features are obvious (Figure 5). Schwertmann (1984b) attributed this to an intermediate goethite phase, with slightly modified unit-cell dimensions, which forms when the domains of goethite crystals are greater than a certain size. The same effect has been observed previously for Al-substituted

https://doi.org/10.1346/CCMN.2010.0580311 Published online by Cambridge University Press

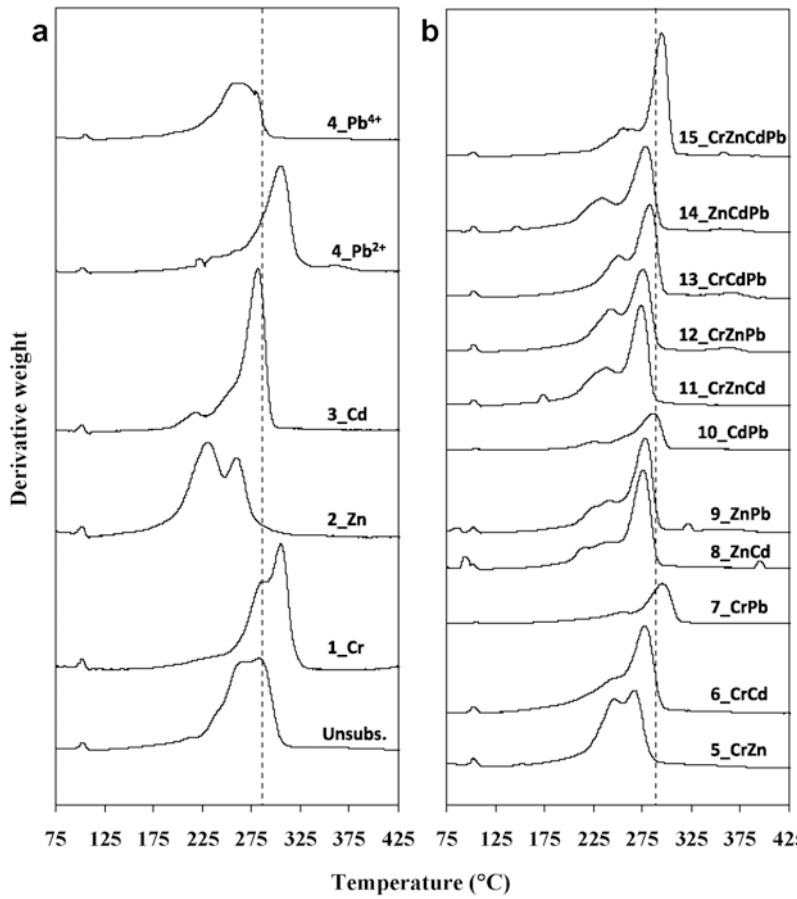

Figure 5. Thermogravimetric analysis curves for (a) pure goethite and single-metal (Cr, Zn, Cd, and Pb)-substituted goethites; (b) di-, tri-, and tetra-metal (Cr, Zn, Cd, and Pb)-substituted goethites. The dashed line indicates the dehydroxylation temperature for pure goethite.

goethite (Forsyth *et al.*, 1968; Jonas and Solymer, 1970; Fey and Dixon, 1981; Schulze and Schwertmann, 1984). The TGA graphs for single Cr-substituted, most di-metal-substituted, and all tri-metal- and tetra-metal-substituted goethite samples exhibited a shoulder on the lower-temperature side of the main peak at ~33–45ºC below the peak (Figure 5b). The pre-treatment of samples with ammonium oxalate also complicates (broadens) the differential thermal analysis pattern due to the decomposition of adsorbed oxalate during heating (Huynh *et al.*, 2003). Ford and Bertsch (1999) attributed the multiple thermal events occurring at 200–260ºC to the decomposition of surface-coordinated OH-groups (=S_1OH, =S_2OH, =S_3OH) and at 270–280ºC to the bulk goethite dehydroxylation. Wells *et al.* (2006) found that bulk dehydroxylation of HCl-treated (used to avoid the effect of ammonium oxalate) Mn-, Ti-, and Al-bearing goethites was characterized by a distinct endotherm doublet. Wells *et al.* (2006) related the first endotherm to the initial phase transformation of goethite to proto-hematite, and the second enotherm to the delayed or inhibited domain growth of protohematite.

The amount of water lost above 150ºC constituted structural OH and ranged from 9.65 to 12.67% w/w, close to the theoretical weight loss of 10.14% w/w for goethite. The structural water loss was unrelated to any morphological or structural property of goethite and is generally greater for all Zn-containing goethites and greatest for singly Zn-substituted goethite, corroborating the intake of extra H^+ as part of a charge-balancing mechanism suggested by Kaur *et al.* (2009a).

Dissolution kinetics of the pure and metal-substituted goethites

After 488 h, dissolution of pure and single-metal-substituted goethites at 40ºC in 1 M HCl occurred in the order: Zn-goethite > Pb-goethite > Pure goethite > Cd-goethite > Cr-goethite (Figure 6a). Zinc-substituted goethite dissolved fully while only a relatively small fraction of the Cr-goethite was dissolved (Table 3). In multi-metal incorporated goethite, the combined influence of the foreign metals on goethite dissolution was observed. In di- and tri-metal incorporated goethites, the presence of Zn together with Cd or Pb or all three

https://doi.org/10.1346/CCMN.2010.0580311 Published online by Cambridge University Press

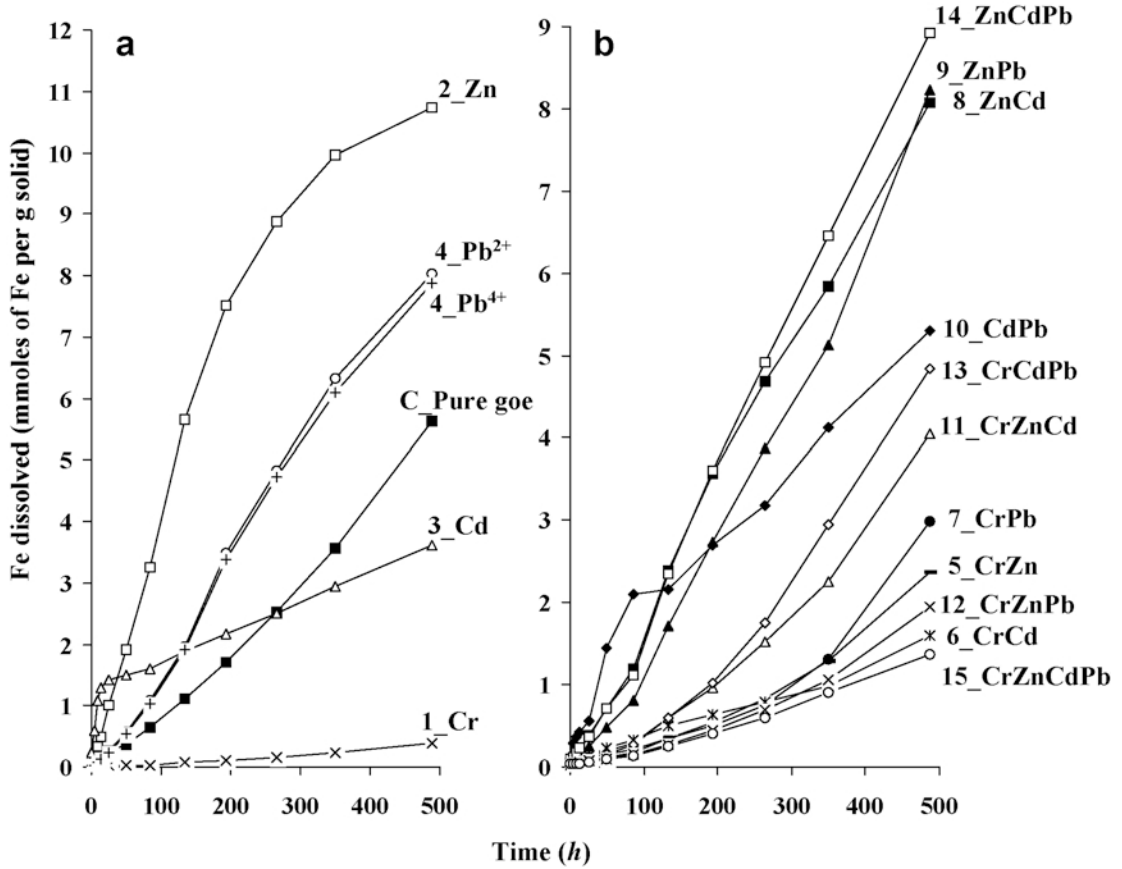

Figure 6. The Fe dissolution-time curves of synthetic single-, di-, tri-, and tetra-metal (Cr, Zn, Cd, and Pb)-substituted goethites and pure goethite.

Table 3. Proportions of Fe, Cr, Zn, Cd, and Pb dissolved from synthetic pure, single-, di-, tri-, and tetra-metal (Cr, Zn, Cd, and Pb)-substituted goethite in 1 M HCl at 40ºC at t = 488 h. The Fe dissolution parameters derived from the Kabai rate law are also given.

Sample	% metal dissolved at t = 488 h					Kabai law Fe dissolution parameters		
	Fe	Cr	Zn	Cd	Pb	x_{Fe}[a]	k_{Fe} ($\times 10^{-3}$) (h^{-1})[b]	SSE[c] ($\times 10^{-3}$)
C_pure goe.	37.9	–	–	–	–	1.42	1.183	0.58
1_Cr	4.1	6.6	–	–	–	1.45	0.223	0.02
2_Zn	100.0	–	99.6	–	–	1.32	5.882	1.92
3_Cd	36.4	–	–	48.6	–	0.37	0.160	6.12
4a_Pb	69.8	–	–	–	72.1	1.39	2.373	0.65
4b_Pb	65.1	–	–	–	74.1	1.34	2.193	0.95
5_CrZn	21.3	32.0	19.3	–	–	1.68	0.861	0.49
6_CrCd	16.3	11.1	–	12.2	–	0.94	0.303	0.51
7_CrPb	33.1	23.2	–	–	27.2	2.35	1.375	1.37
8_ZnCd	80.3	–	73.4	80.4	–	1.36	2.744	2.59
9_ZnPb	73.2	–	67.9	–	97.8	1.62	2.283	4.35
10_CdPb	52.2	–	–	35.3	33.4	0.74	1.205	5.56
11_CrZnCd	46.2	36.1	38.2	36.7	–	1.81	1.542	1.41
12_CrZnPb	21.6	18.8	19.2	–	58.7	1.71	0.885	0.28
13_CrCdPb	50.5	38.6	–	38.9	86.4	1.94	1.706	0.48
14_ZnCdPb	86.3	–	71.7	94.6	100.6	1.45	2.615	2.05
15_CrZnCdPb	14.4	19.6	13.5	14.9	50.0	1.35	0.516	0.11

[a] x_{Fe}: characteristics of the structure of the solid phase, [b] k_{Fe}: dissolution rate, h^{-1}; [c] SSE: sum of standard errors.

https://doi.org/10.1346/CCMN.2010.0580311 Published online by Cambridge University Press

together, increased goethite dissolution (73–86%, Figure 6b, Table 3). In contrast, the presence of Cr suppressed the dissolution of Zn, Pb, and Cd containing di-metal-substituted goethites by more than two-fold (16–33% in the order: Pb > Zn > Cd) (Figure 6b, Table 3). In tri- and tetra-metal-incorporated goethites, the presence of Cr with Zn, Cd, and Pb decreased goethite dissolution to 14–50% (Figure 6b, Table 3).

Of all the single- and multi-metal-substituted and pure goethite samples studied, singly Zn-substituted goethite dissolved most rapidly and singly Cr-substituted goethite dissolved most slowly. Stabilization of goethite by Cr and Al was noted by Schwertmann *et al.* (1989). Lim-Nunez and Gilkes (1987), on the basis of unit surface area, showed that Cr-substituted goethite dissolved at about one-tenth of the rate of unsubstituted, Ni- and Al-goethites (3 g Fe/m^2/h), whereas Co- and Mn-goethites dissolved at about twice that rate.

The Fe-dissolution data of all single- and multi-metal-substituted and pure goethites were fitted to the Kabai rate law (Kabai, 1973), as given below:

$$1 - \alpha = e^{-(kt)x}$$

where α is the fraction of Fe dissolved at time t, and k and x are Kabai equation coefficients representing the dissolution-rate constant and the characteristics of the structure of the solid phase, respectively. Kabai plots for selective samples are shown in Figure 7.

The Fe-dissolution rate constant (k_{Fe}) ranged from $(0.16 \text{ to } 5.88) \times 10^{-3}$ h^{-1} for single- and multi-metal-substituted and pure goethite (Table 3). The k_{Fe} value was greatest (5.88×10^{-3} h^{-1}) for Zn-substituted goethite and smaller for Cr-, Cd-, and (Cr,Zn)-substituted goethite, $(0.160 \text{ to } 0.303) \times 10^{-3}$ h^{-1} (Table 3). The values of k_{Fe} were generally greater ($(2.28 \text{ to } 2.74) \times 10^{-3}$ h^{-1}) for Pb, ZnCd, ZnPb, and ZnCdPb than for pure goethite, indicating destabilization of goethite *vs*. proton attack (Table 3). Goethite containing Cr, co-substituted with Cd, Pb, and Zn, had small k_{Fe} values at $(0.516 \text{ to } 1.706) \times 10^{-3}$ h^{-1} (Table 3). In di-metal substituted goethites, co-incorporation of Cr or Cd with

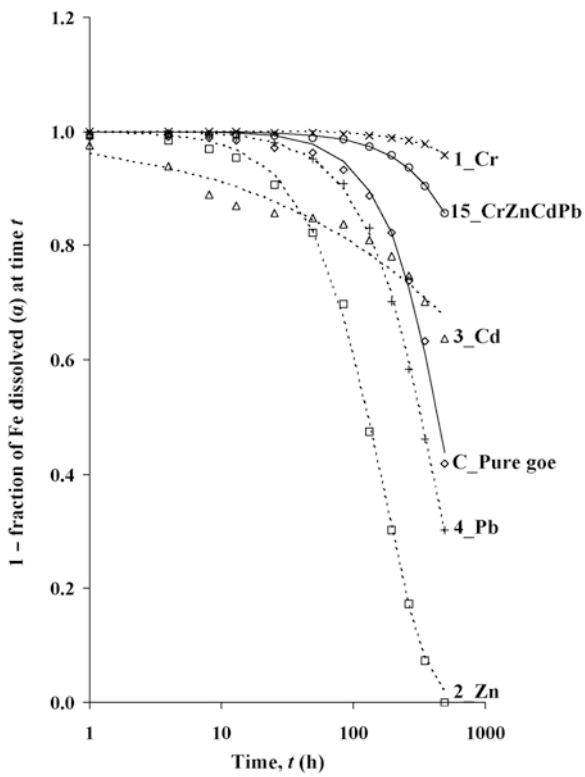

Figure 7. Kabai plots for synthetic single- and tetra-metal (Cr, Zn, Cd, and Pb)-substituted and pure goethites.

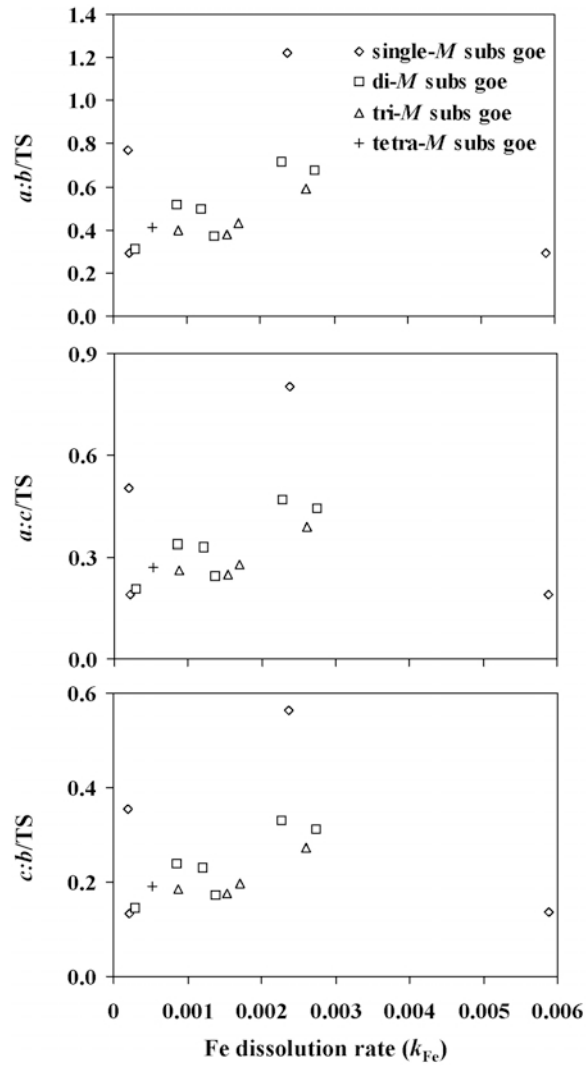

Figure 8. Relation between dissolution rates of synthetic single-, di-, tri-, and tetra-metal (Cr, Zn, Cd, and Pb)-substituted goethites *vs.* steric strains *a*:*b*, *a*:*c* and *c*:*b* per unit total metal substitution.

https://doi.org/10.1346/CCMN.2010.0580311 Published online by Cambridge University Press

Zn suppressed k_{Fe} as compared to single-Zn-substituted goethite by 85 and 53%, respectively (Table 3). Conversely, the co-incorporation of Zn along with Cr or Cd in goethite increased k_{Fe} as compared to single Cr- or Cd-substituted goethite by 286 and 1615%, respectively (Table 3). CrZn-substituted goethite had a smaller k_{Fe} and (Zn,Cd)-substituted goethite had a larger k_{Fe} value than that of pure goethite (Table 3). Similarly, co-incorporation of Cr or Cd with Pb(II) in goethite suppressed the k_{Fe} compared to single Pb(II)-substituted goethite by ~50% (Table 3). Conversely, the co-incorporation of Pb(II) along with Cr or Cd in goethite increased the k_{Fe} as compared to single Cr- or Cd-substituted goethite by 516 and 653%, respectively (Table 3). Both, (Cr,Pb)- and (Cd,Pb)-substituted goethites had slightly larger k_{Fe} values than that of pure goethite (Table 3). The results suggest that Cd and, in particular Cr, suppressed the destabilization of goethite induced by the incorporation of Zn and Pb, making goethite more resistant to proton attack. The results also suggest that inclusion of Pb and, in particular Zn, acted to offset the stabilizing effect of Cr and Cd on goethite.

The k_{Fe} values of multi-metal-substituted goethites generally increased with structural strain caused per unit of total metal substitution (Figure 8). Single-metal-substituted goethite (excluding Cr-substituted goethite) did not follow this trend. Structural strain was defined along each crystallographic direction by the ratios of various unit-cell dimensions (*a*:*b, a*:*c, c*:*b*). In spite of the greater structural strain per unit of total metal substitution, in the case of Pb(IV) (3.29), Pb(II) (1.22), and Cd (0.76) goethites compared to Zn-goethite (0.29), the k_{Fe} of Pb(IV), Pb(II), and Cd goethites were smaller ($\leqslant 0.003\ h^{-1}$) than Zn goethite ($0.006\ h^{-1}$). The k_{Fe} appears to be related to the local coordination environments around substituent metals, which is highly distorted around Zn as compared to other metals (Kaur *et al.*,

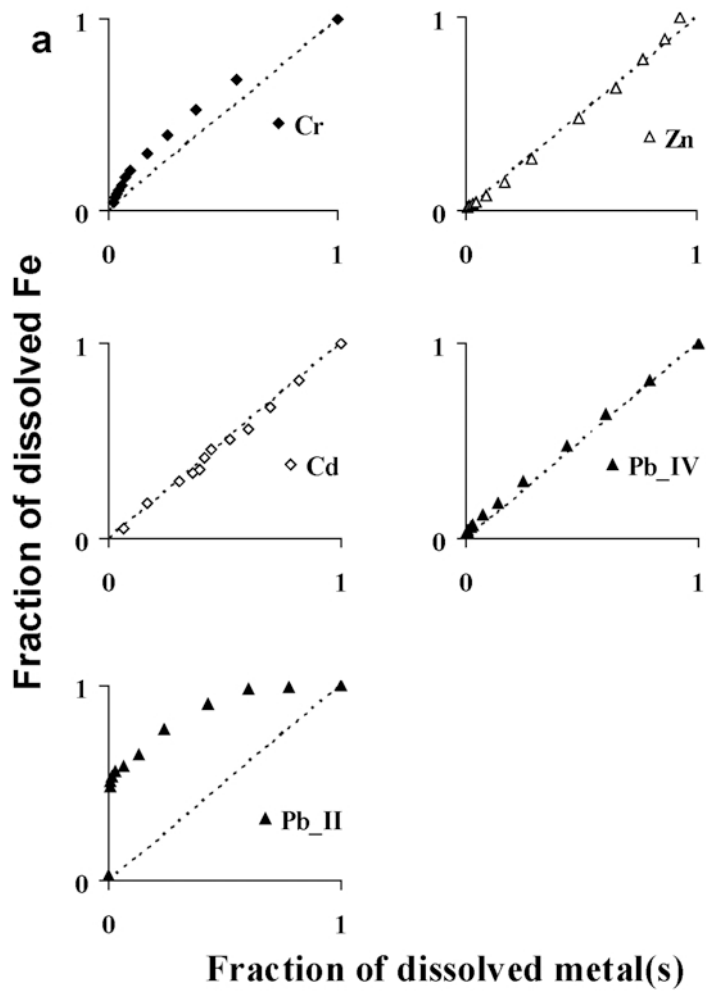

Figure 9. Congruency of Fe and metal(s) dissolution in synthetic (a) (*above*) single-, (b) (*facing page*) di-, tri-, and tetra-metal (Cr, Zn, Cd, and Pb)-substituted goethites. All Pb in di-, tri-, and tetra-metal (Cr, Zn, Cd, and Pb)-substituted goethites is divalent.

https://doi.org/10.1346/CCMN.2010.0580311 Published online by Cambridge University Press

2009a). The greater rate of dissolution of single- and multi-metal (Zn)-substituted samples could be attributed to the greater structural disorder in the goethite structure caused by the replacement of Fe by Zn.

The stability against proton attack of goethite containing only Cr or Cr in combination with other metals may be due to the formation of broader lath-shaped crystals with well developed (100) faces compared to narrow, lath-shaped crystals formed where Zn/Pb/Cd substitute for Fe, either singly or all together, in goethite (Figure 1a,b). Cornell *et al.* (1974) found the dissolution of synthetic goethite crystals to be

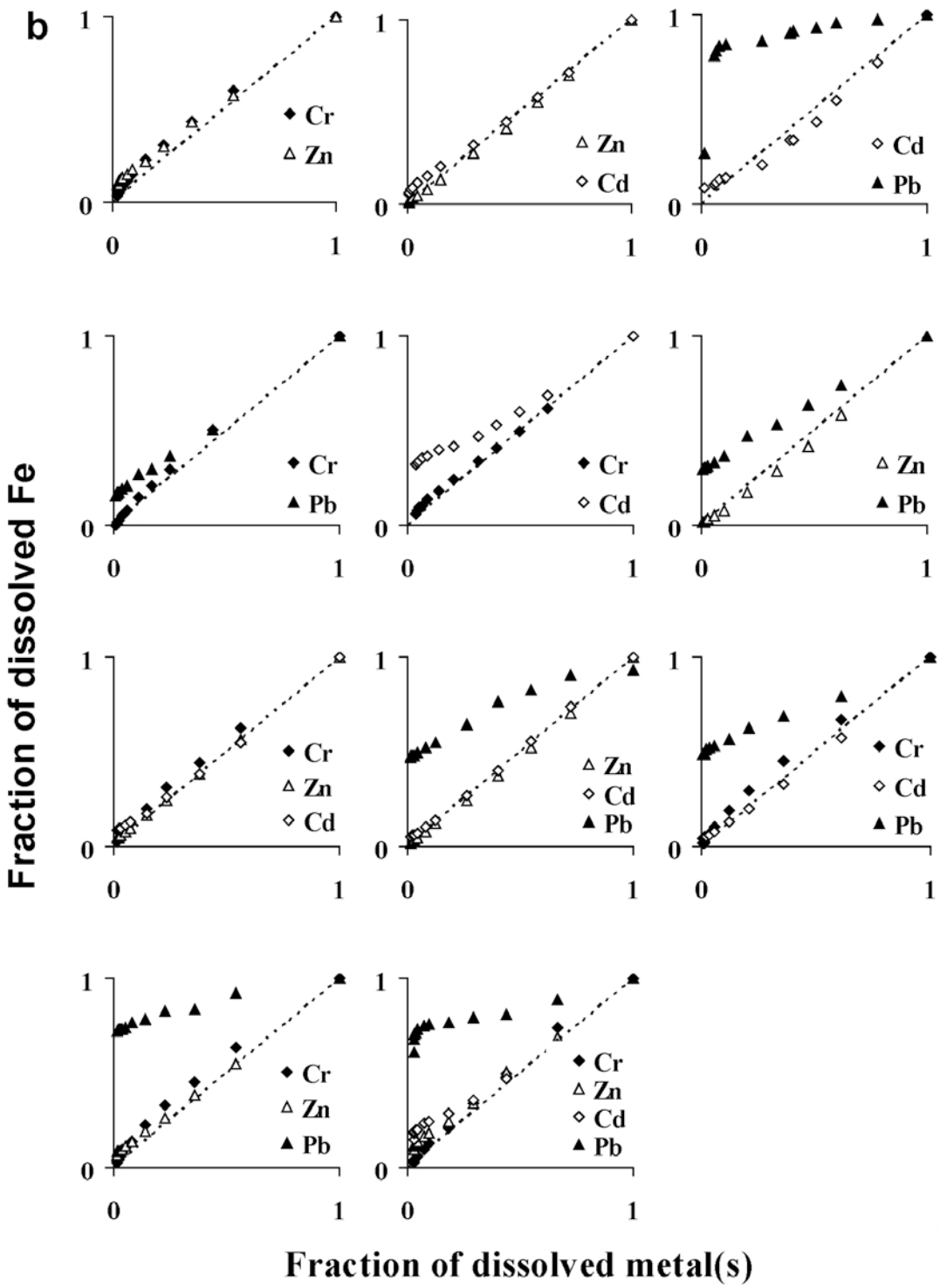

https://doi.org/10.1346/CCMN.2010.0580311 Published online by Cambridge University Press

anisotropic; the (010) and (001) faces dissolve more rapidly than the (100) face. The reason for this, suggested by Cornell *et al.* (1974), was that all triply, doubly, and singly coordinated hydroxyl groups occur on the (100) face, whereas doubly and singly coordinated hydroxyl groups occur on the (010) face and only singly coordinated hydroxyl groups occur on the (001) face. Accordingly, the broader lath-shaped crystals of Cr(+*M*)-bearing goethite are expected to contain a greater proportion of triply coordinated hydroxyls, which would be the most difficult to remove from the crystal surface and would, thus, decrease the dissolution rate.

Singly Cr-substituted goethite and multi-metal-substituted goethites where one of the metals is Cr developed rough surfaces or serrated edges after treatment with 0.2 M oxalic acid/ammonium oxalate used to remove any amorphous phases (Figure 1). Lim-Nunez and Gilkes (1987) observed similar effects after treatment with the same solution. The rough surface might provide points susceptible to HCl dissolution. Lim-Nunez and Gilkes (1987) observed extensive development of etchpits for Cr goethite during dissolution in HCl and also much larger frequency factors for Cr goethite (10^{-16} to 10^{-14} g Fe/m^2/h). Those authors found, however, that the large frequency factors were insufficient to counteract the effect of the largest activation energies (21–33 kcal/mol) for Cr goethite, leading to their smallest dissolution rate.

One of the reasons for the rapid dissolution of Zn-substituted goethite compared with other metal-bearing goethites could be the widening of openings along the (001) face and tunnels as a result of breakage of H-bonds due to incorporation of distorted Zn octahedra (Kaur *et al.*, 2009a). Cornell *et al.* (1974) suggested that the (001) face had a more open structure than other faces and that tunnels ~4 Å^2 in area run through the crystal parallel to the (001) axis (Gallagher and Phillips, 1968). The latter authors suggested that tunnel openings on the (001) face enable protons to approach the surface much more closely than elsewhere. Moreover, diffusion of protons through the tunnels is fairly rapid and the whole tunnel (not just its opening) may be involved in the later stages of reaction when crystals start to disintegrate (Gallagher and Phillips, 1968). Similarly, addition of Pb is expected to result in some degree of opening of the goethite structure, locally or at the unit-cell scale (Kaur *et al.*, 2009a), which may assist in the dissolution of Pb-substituted goethites. In contrast, some local and unit-cell contractions were observed in Cr-substituted goethite as compared to pure goethite (Schwertmann *et al.*, 1989; Kaur *et al.*, 2009a) which could increase resistance to proton attack. Also, the symmetric Cr/Cd octahedra as compared to asymmetric Zn/Pb octahedra appear to provide more stability against proton attack. The results show that the local and extended coordinations around the substituent metal(s), not the ionic radii, control the dissolution properties of metal-substituted goethite.

Congruency of metal(s) dissolution with Fe

The congruency of metal(s) and Fe dissolution as goethite dissolves provides important information regarding the distribution of metal(s) within crystals (Singh and Gilkes, 1992; Wells, 1997; Landers and Gilkes, 2007). The congruency is indicated by a line of unit slope for plots of %metal *vs*. %Fe dissolved, as the line of unit slope indicates that both Fe and the metal are uniformly distributed (*e.g.* Figure 9). If the metal(s) and Fe dissolve at a similar rate, the metal is distributed uniformly throughout the crystals. On the contrary, if the substituted metals dissolve faster (above the unit line) or slower (below the unit line) than Fe, metals are concentrated at the crystal periphery or toward the core, respectively. Heterogeneous dissolution may also indicate the presence of another mineral phase.

Dissolution studies showed that Cr, Zn, and Cd dissolved congruently to Fe, whether present in single- or multi-metal-substituted goethites (Figure 9a,b), indicating that these metals were distributed homogeneously in the goethite crystals. Tetravalent Pb, present in single Pb-substituted goethite (sample Pb_IV, Figure 9a), dissolved congruently with Fe, suggesting that Pb(IV) was incorporated homogeneously into the bulk structure. In contrast, divalent Pb, either in single- or multi-metal-substituted goethites, dissolved at a much faster rate than Fe (Figure 9a,b), indicating that most of the Pb(II) was enriched in the near-surface region. All Pb, either in single- or multi-metal-substituted goethites is divalent, except the sample indicated as Pb_IV. Kaur *et al.* (2009a) observed that the local coordination of Pb(II) and Pb(IV) were similar and contained three Pb–*M* distances similar to those present in the bulk goethite structure. The only significant difference was that the corner-sharing Pb–*M* distance was greater for Pb(II) than for either Pb(IV) or pure goethite itself. The apparent inconsistency between the present dissolution and previous XAFS results could be attributed to smaller Pb(IV) (0.775 Å) compared to the larger Pb(II) (1.19 Å). Whereas Pb(IV) would be easily accepted by the growing goethite units with distribution approaching uniformity, Pb(II) would concentrate at the surface of goethite crystals.

CONCLUSIONS

The morphology, dehydroxylation temperature, and dissolution stability of single- and multi-metal (Cr, Zn, Cd, and Pb)-substituted goethites were interrelated and strongly dependent on the structural properties of goethite. The dissolution properties of goethites were mainly determined by the local coordination environment, rather than directly by ionic radii and valence of the substituent metals, suggesting the need to study

https://doi.org/10.1346/CCMN.2010.0580311 Published online by Cambridge University Press

changes in the goethite structure at the local scale. The same was true for morphological and dehydroxylation properties of the mineral. The effects of the substituent metals on goethite structure and its properties were similar in single- and multi-metal systems. The effects of individual metals were not cumulative in multi-metal systems; certain metals had more control on the structure and properties of goethite. This changed the whole scenario that would otherwise have been expected based on studies of single-metal systems. The situation became complicated as different properties were influenced by different metals. For example, destabilization of goethite against H^+ attack caused by incorporation of Zn could be negated by the addition of Cr. However, the presence of Cr only partially moderated the decrease in the thermal stability resulting from the incorporation of Zn. The present study clearly demonstrates the need to extend studies of metal substitution in goethite from single-metal systems to multi-metal systems in order to better understand the complex behavior of naturally occurring Fe oxides.

ACKNOWLEDGMENTS

This study was supported by an Australian Research Council Discovery Grant (DP0558332). Navdeep Kaur gratefully acknowledges Shaun Bulcock for his help with the TEM analysis, Dr De Bruyn Hank for training in TGA, and appreciates the funding of her PhD scholarship by the Department of Education, Science and Training through the Endeavour International Postgraduate Research Scholarship and University of Sydney through the International postgraduate award.

REFERENCES

Alvarez, M., Sileo, E.E., and Rueda, E.H. (2005) Effect of Mn (II) incorporation on the transformation of ferrihydrite to goethite. *Chemical Geology*, **216**, 89–97.

Alvarez, M., Rueda, E.H., and Sileo, E.E. (2007) Simultaneous incorporation of Mn and Al in the goethite structure. *Geochimica et Cosmochimica Acta*, **71**, 1009–1020.

Atkinson, R.J., Posner, A.M., and Quirk, J.P. (1968) Crystal nucleation in Fe(III) solutions and hydroxide gels. *Journal of Inorganic and Nuclear Chemistry*, **30**, 2371–2374.

Cambier, P. (1986) Infrared study of goethites of varying crystallinity and particle size: I. Interpretation of OH and lattice vibration frequencies. *Clay Minerals*, **21**, 191–200.

Clay Minerals Society (CMS) Nomenclature Committee (1971) Summary of national and international recommendations on clay mineral nomenclature. *Clays and Clay Minerals*, **19**, 129–132.

Cornell, R.M., Posner, A.M., and Quirk, J.P. (1974) Crystal morphology and the dissolution of goethite. *Journal of Inorganic and Nuclear Chemistry*, **36**, 1937–1946.

Dudka, S. and Adriano, D.C. (1997) Environmental impacts of metal ore mining and processing: A review. *Journal of Environmental Quality*, **26**, 590–602.

Fey, M.V. and Dixon, J.B. (1981) Synthesis and properties of poorly crystalline hydrated aluminous goethites. *Clays and Clay Minerals*, **29**, 91–100.

Ford, R.G. and Bertsch, P.M. (1999) Distinguishing between surface and bulk dehydration-dehydroxylation reactions in synthetic goethites by high-resolution thermogravimetric analysis. *Clays and Clay Minerals*, **47**, 329–337.

Forsyth, J.B., Hedley, J.G., and Johnson, C.E. (1968) The magnetic structure and hyperfine field of goethite (α-FeOOH). *Journal of Physics*, **C1**, 179–188.

Gallagher, K.J. and Phillips, D.N. (1968) Proton transfer studies in the ferric oxyhydroxides. Part1. Hydrogen exchange between alpha-FeOOH and water. *Transactions of the Faraday Society*, **64**, 785–795.

Gerth, J. (1990) Unit cell dimensions of pure and trace metal-associated goethites. *Geochimica et Cosmochimia Acta*, **54**, 363–371.

Goss, C.J. (1987) The kinetics and reaction mechanism of the goethite to hematite transformation. *Mineralogical Magazine*, **51**, 437–451.

Huynh, T., Tong, A.R., Singh, B., and Kennedy, B.J. (2002) Studies of synthetic copper containing goethite. In: *17th World Congress of Soil Science, Bangkok, Thailand, 14–20 August 2002*.

Huynh, T., Tong, A.R., Singh, B., and Kennedy, B.J. (2003) Cd-substituted goethites – A structural investigation by synchrotron X-ray diffraction. *Clays and Clay Minerals*, **51**, 397–402.

Jonas, K. and Solymer, K. (1970) Preparation, X-ray, derivatographic and infrared study of aluminium substituted goethites. *Acta Chimica Academiae Scientiarum Hungaricae*, **66**, 383–394.

Kabai, J. (1973) Determination of specific activation energies of metal oxides and metal oxide hydrates by measurement of the rate of dissolution. *Acta Chimica Academiae Scientiarum Hungaricae*, **78**, 57–73.

Kaur, N., Grafe, M., Singh, B., and Kennedy, B.J. (2009a) Simultaneous incorporations of Cr, Zn, Cd and Pb in the goethite structure. *Clays and Clay Minerals*, **57**, 234–250.

Kaur, N., Singh, B., Kennedy, B.J., and Grafe, M. (2009b) The preparation and characterization of vanadium substituted goethite: the importance of temperature. *Geochimica et Cosmochimia Acta*, **73**, 582–593.

Landers, M. and Gilkes, R.J. (2007) Dehydroxylation and dissolution of nickeliferous goethite in New Caledonian lateritic Ni ore. *Applied Clay Science*, **35**, 162–172.

Lim-Nunez, R. and Gilkes, R.J. (1987) Acid dissolution of synthetic metal containing goethites and hematites. Pp. 197–204 in: *Proceedings of the International Clay Conference, Denver, 1985* (L.G. Schultz, H. van Olphen and F.A. Mumpton, editors). The Clay Minerals Society, Bloomington, Indiana, USA.

Luo, Y.-R. and Kerr, J.A. (2006–2007) Bond dissociation energies. In: *CRC Handbook of Chemistry and Physics* (D.R. Lide, editor). Taylor and Francis, Boca Raton, Florida, USA.

Manceau, A., Schlegel, M.L., Musso, M., Sole, V.A., Gauthier, C., Petit, P.E., and Trolard, F. (2000) Crystal chemistry of trace elements in natural and synthetic goethite. *Geochimica et Cosmochimica Acta*, **64**, 3643–3661.

Primentel, G.C. and McClellan, A.L. (1960) *The Hydrogen Bond*. W.H. Freeman and Company, San Francisco, London.

Ressler, T. (1998) WinXAS: a program for x-ray absorption spectroscopy data analysis under MS-Windows. *Journal of Synchrotron Radiation*, **5**, 118–122.

Ruan, H.D. and Gilkes, R.J. (1995) Acid dissolution of synthetic aluminous goethite before and after transformation to hematite by heating. *Clay Minerals*, **30**, 55–65.

Schulze, D.G. and Schwertmann, U. (1984) The influence of aluminium on iron oxides. X. Properties of Al-substituted goethites. *Clay Minerals*, **19**, 521–539.

Schulze, D.G. and Schwertmann, U. (1987) The influence of aluminum on iron-oxides. 13. Properties of goethites synthesized in 0.3 M KOH at 25-Degrees-C. *Clay Minerals*, **22**, 83–92.

Schwarzmann, E. and Sparr, H. (1969) Die Wasserstoff-

bruckenbindung in Hydroxiden mit Diasporstruktur. *Zeitschrift für Naturforschung*, **24b**, 8–11.

Schwertmann, U. (1984a) The influence of aluminium on iron oxides: IX. Dissolution of Al-goethites in 6M HCl. *Clay Minerals*, **19**, 9–19.

Schwertmann, U. (1984b) The double dehydroxylation peak of goethite. *Thermochimica Acta*, **78**, 39–46.

Schwertmann, U. (1991) Solubility and dissolution of iron-oxides. *Plant and Soil*, **130**, 1–25.

Schwertmann, U., Cambier, P., and Murad, E. (1985) Properties of goethites of varying crystallinity. *Clays and Clay Minerals*, **33**, 369–378.

Schwertmann, U., Gasser, U., and Sticher, H. (1989) Chromium-for-iron substitution in synthetic goethites. *Geochimica et Cosmochimica Acta*, **53**, 1293–1297.

Shannon, R.D. (1976) Revised effective ionic radii and systematic studies of interatomic distances in halides and chalcogenides. *Acta Crystallographica*, **A32**, 751–767.

Sileo, E.E., Ramos, A.Y., Magaz, G.E., and Blesa, M.A. (2004) Long-range vs. short-range ordering in synthetic Cr-substituted goethites. *Geochimica et Cosmochimica Acta*, **68**, 3053–3063.

Singh, B. and Gilkes, R.J. (1992) Properties and distribution of iron oxides and their association with minor elements in the soils of south-western Australia. *Journal of Soil Science*, **43**, 77–98.

Singh, B., Sherman, D.M., Gilkes, R.J., Wells, M.A., and Mosselmans, J.F.W. (2002) Incorporation of Cr, Mn and Ni into goethite (alpha-FeOOH): mechanism from extended X-ray absorption fine structure spectroscopy. *Clay Minerals*, **37**, 639–649.

Stiers, W. and Schwertmann, U. (1985) Evidence for manganese substitution in synthetic goethite. *Geochimica et Cosmochimica Acta*, **49**, 1909–1911.

Vega, F.A., Covelo, E.F., Andrade, M.L., and Marcet, P. (2004) Relationships between heavy metals content and soil properties in minesoils. *Analytica Chimica Acta*, **524**, 141–150.

Wells, M.A. (1997) Mineral, chemical and magnetic properties of synthetic, metal-substituted goethite and hematite. Ph.D. thesis, University of Western Australia.

Wells, M.A., Fitzpatrick, R.W., and Gilkes, R.J. (2006) Thermal and mineral properties of Al-, Cr-, Mn-, Ni- and Ti-substituted goethite. *Clays and Clay Minerals*, **54**, 176–194.

Wilcox, D., Dove, B., McDavid, D., and Greer, D. (1995) *UTHSCASA Image Tool for Windows*. The University of Texas Health Science Centre, San Antonio, Texas, USA.

(*Received 21 October 2008; revised 27 April 2010; Ms. 217; A.E. S. Petit*)